2D finite element inundation modelling in anabranching channels with sparse data: examination of uncertainties

Joy Sanyal, Alexander L. Densmore and Patrice Carbonneau

Department of Geography
Durham University, Durham, U.K.

Address:
Department of Geography
Durham University,
Science Laboratories
South Road, Durham
DH1 3LE, U.K.

Email: sanyal.j@gmail.com
Phone: 44 (0) 191 33 41949
Fax: +44 (0) 191 33 41801

Abstract

Flood inundation modelling in developing countries is severely limited by the lack of high resolution terrain data and suitable imagery to map flood extents. This study assessed the predictive uncertainty of modelled flood extents generated from TELEMAC2D model using low-cost, sparse input data commonly available in developing countries. We studied a river reach characterised by anabranching channels and river islands in eastern India. In this complex fluvial setting, we analysed computational uncertainty as a function of error in both satellite-derived flood-extent maps using a Generalised Likelihood Uncertainty Estimation (GLUE)-based approach. The model performance was quite sensitive to the uncertainty in the inflow hydrograph, particularly close to the flood peak. Evaluation of the flood inundation probability map, conditioned upon deterministic and probabilistic observed flood extents, reveals that the effect of using probabilistic observed data is only evident for portions of the model domain where the model output is free from consistent bias (over or under prediction) likely created by the imperfect terrain data.

Keywords: Uncertainty, finite element inundation model, sparse data, TELEMAC2D, GLUE, high performance computing

1 Introduction

Flooding is one of the most serious natural hazards and disproportionately affects the global south due to extreme precipitation events associated with tropical cyclones and monsoon bursts (Adhikari et al., 2010). Accurate assessment of flood extent for a given river discharge requires a flood inundation model, which in turn depends upon topography along with upstream and downstream boundary discharge/stages. Such models are often calibrated and validated against inundation extents derived from satellite data (e.g., Horritt, 2000) and gauged water levels (e.g., Pappenberger et al., 2005). Most of the required data mentioned above are either non-existent or of poor quality in many developing countries (Patro et al., 2009). In these data-sparse areas, modelled inundation maps suffer from uncertainties in (1) estimated discharge from stage-discharge relationships (Di Baldassarre and Claps, 2011; Di Baldassarre and Montanari, 2009), (2) topography, (3) assumed state in the model (e.g. steady versus unsteady), (4) boundary roughness parameterization, (5) calibration and validation data, and (6) choice of model (1D versus 2D) (Jung and Merwade, 2012; Bales and Wagner, 2009). Whilst the uncertainty arising from model choice and structure (i.e. different combinations of internal parameters and the way they are linked) is a global issue, uncertainties arising from poor-quality inputs are much more pronounced in data-sparse regions. Such uncertainties can combine in unforeseen ways. For example, while the overall uncertainty in flood risk estimation emanates from superimposition of number of sources (Merz et al., 2008), Jung and Merwade (2012) found that topographic uncertainty made the model outputs less sensitive to inflow hydrograph uncertainty.

Generalised Likelihood Uncertainty Estimation (GLUE) by Beven and Binley (1992) is the most widely used framework for hydrological uncertainty assessment (Montanari, 2006). The GLUE procedure searches for sets of parameter values that would give reasonably accurate model outputs for a range of model inputs. This method does not require the modeller to maximize any objective performance measure for the model. Instead, it derives the performance of parameter sets from a likelihood or goodness-of-fit index that broadly resembles the concept of probability.

With the increased availability of remotely-sensed data to capture the extent of inundation, binary flood maps have been used to quantify the distributed uncertainty of inundation models under the GLUE approach (Aronica et al., 2002). Recognizing the possibility of error in these

maps, Schumann et al. (2009) proposed ‘possibility of inundation’ maps rather than deterministic binary flood maps. Di Baldassarre et al. (2009) used this concept to propose a method for generating GLUE-based 'flood uncertain inundation maps'. Stephens et al. (2012) noted that the selection of uncertain observed data from different areas of the model domain can result in considerable differences in overall uncertainties in the inundation modelling outcomes.

Although 1D hydrodynamic models such as HEC-RAS and computationally efficient 1D-2D coupled models like LISFLOOD-FP have been widely used to assess predictive uncertainty, application of fully 2D models for this purpose is rare, likely due to the high computational cost of running a fully 2D model in a Monte Carlo framework (Merz et al., 2008) and the availability of very high resolution topographic data that favours the use of simple models (Bates, 2012) . Fully 2D finite element flood inundation models such as TELEMAC2D are physically realistic and have certain advantages. They are suitable for terrain data with varying resolution (Di Baldassarre et al., 2010) and are less sensitive to uncertainties in the terrain data (Cook and Merwade, 2009), making them more suitable for settings without high-resolution DEMs. In addition, TELEMAC2D was found to be less sensitive to the roughness parameterisation (Horritt, 2000) and shows slower drop off in performance with increasing difference from calibrated ‘optimum’ parameters (Di Baldassarre et al., 2010). Sanyal et al. (2014) showed that a complex model such as TELEMAC2D is more appropriate than 1D-2D models for simulating floodplain inundation for complicated anabranching channel networks and low-quality input data.

Here, we estimate the predictive uncertainty of a computationally-demanding 2D finite element flood inundation model in an anabranching reach at the highest possible resolution with coarse model inputs. Our approach is novel because we explicitly consider inaccuracies in the observed validation data and their effect on uncertainty estimation, and we explore whether this consideration is important for modelling in data-sparse environments.

2 Study Area

The study area was the lower Damodar River, a tributary of the Hoogly River in the Ganges basin, in West Bengal, India (Fig 1). This area is typical of many rivers in the global South. It suffers from frequent flooding during the monsoon season and has very limited availability of the

datasets that are normally required for inundation modelling. The Mundeswari River, one of the main branches of the lower Damodar River, is characterised by numerous channel bifurcations, loops, and a major river island. The area is extremely flat with a relief of only 10 to 12 m over the model scale. Riverbed material is mostly sand and clay while paddy field is the dominant land-use type in the floodplain. Although the study area is mostly drained by the Mundeswari River and its branches, during major floods some portion of the eastern and western boundary of this area experience influx of moderate amounts of flood water from adjacent river basins.

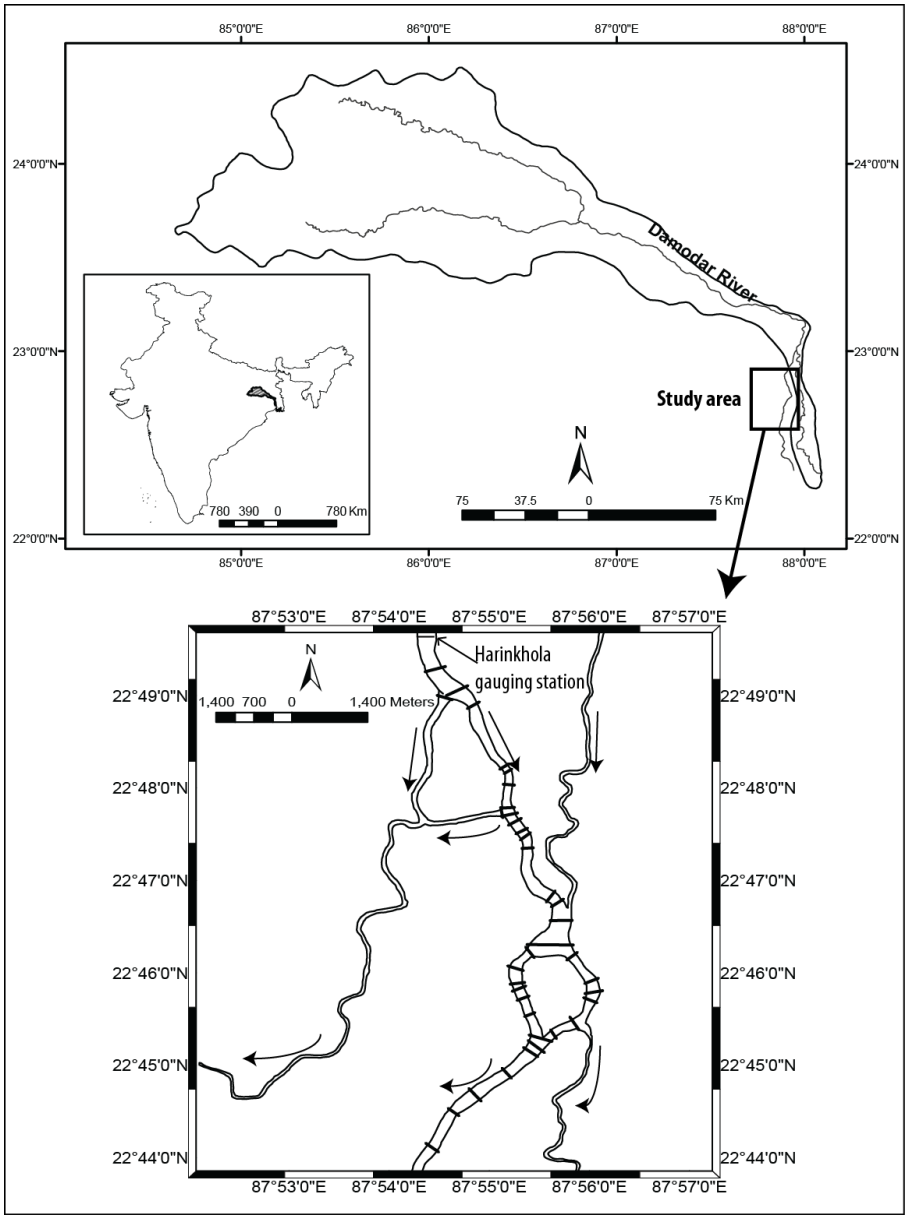

Fig 1 Study area. Inset in the top panel shows the location of the Damodar Basin in India. Locations of the surveyed cross-sections on the main channel are shown in the lower panel.

3 Data and Methods

3.1 Terrain and hydrologic inputs

Low-cost IRS Cartosat-1 panchromatic stereo images (2.5 m spatial resolution), surveyed cross-sections and SRTM DEM were used to create a hybrid terrain data set (Fig 2), following Sanyal et al. (2014). The terrain data was characterised by higher details for the channels, roads, canals and other narrow but hydraulically significant features with progressively lower resolution towards the floodplain.

The hydrological data at Harinkhola gauging station, at the upstream boundary of the model comprise hourly river stages but lack a rating curve. The stage data were converted into discharge (Herschey, 1998) using Manning's equation:

$$Q = \frac{1}{n} R^{a} S^{0.5} \qquad (1)$$

where R is the hydraulic radius (m), a is an exponent, n is Manning's roughness coefficient and S is the bed slope (mm^{-1}). The hydraulic radius and bed slope were derived from a surveyed cross-section at the gauging station. The uncertainty in the discharge figures derived with this method stems mostly from uncertainty in Manning's *n* values for the channel and floodplain at the gauging site.

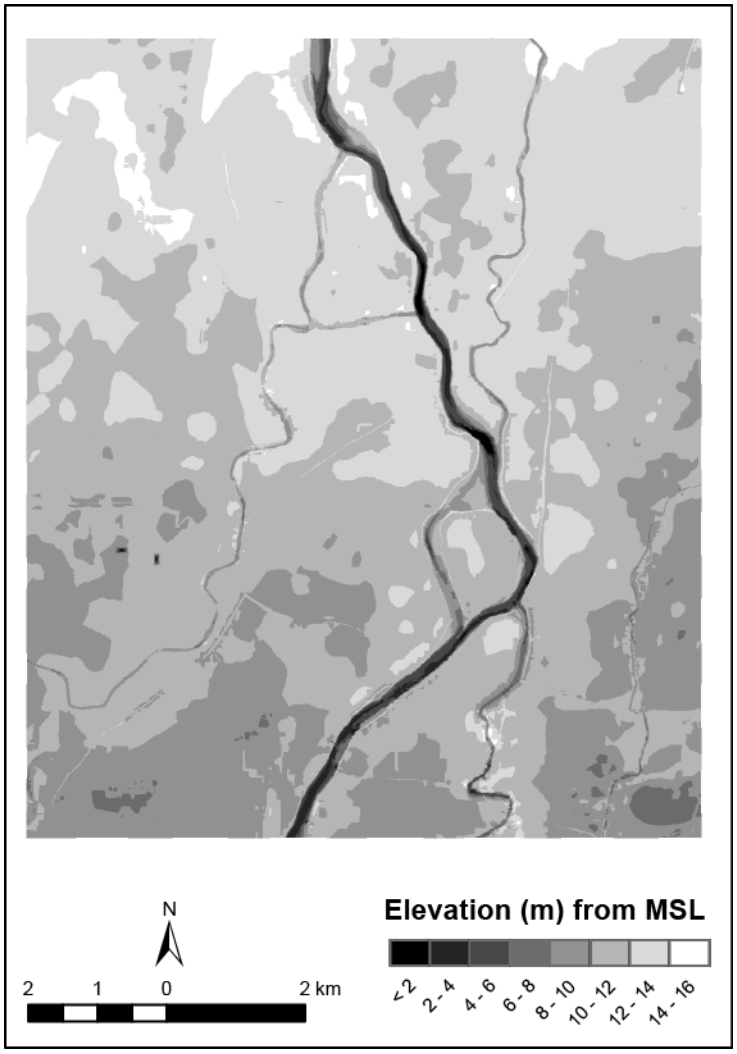

Fig 2 The hybrid terrain data resampled to a 10 m grid for the study area shown in the bottom panel of Fig 1.

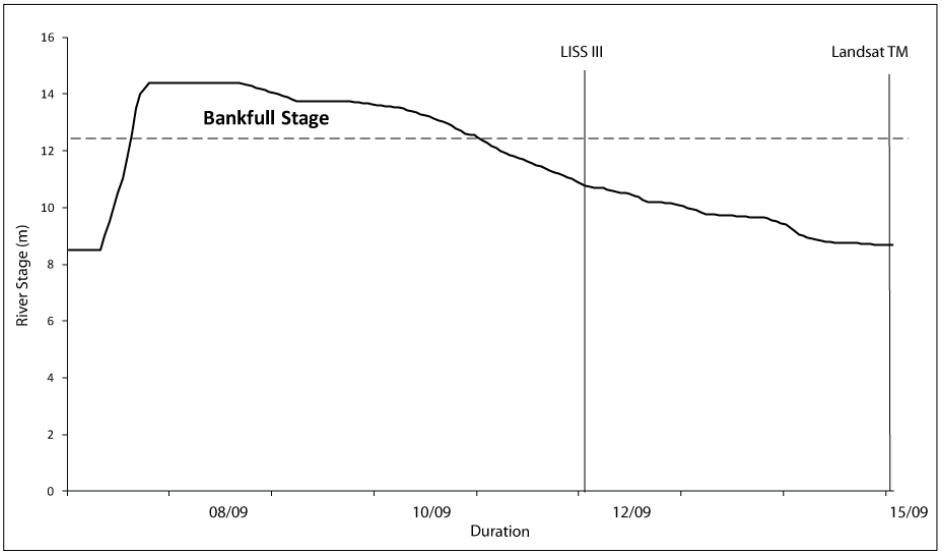

Fig 3 The hydrograph of river stage at Harinkhola gauging station at the model inlet and the acquisition times of two satellite images that were used for model validation.

3.2 Preparing the distributed calibration and validation data

A flood event on 8-15 September 2009 was used for uncertainty assessment. With no available radar images, we used two cloud-free multispectral satellite images from IRS Resourcesat-1 LISS-III (24 m spatial resolution) and Landsat 5 TM for 12 and 15 September, 2009 respectively. The satellite overpass times with respect to the inflow hydrograph are presented in Fig 3. Henceforth, the performance of the flood-inundation model at these two times will be referred to as model states 1 and 2, respectively. To extract inundation extents, we used four methods: supervised and unsupervised classification, NDVI and NDWI. Normalized Difference Vegetation Index (NDVI), computed as (Near Infrared - Red) / (Near Infrared + Red) has been commonly used for differentiating flooded area from dry surface (Jain et al., 2006). Likewise, Normalized Difference Water Index (NDWI), developed by McFeeters (1996) and calculated as (Green - Near Infrared) / (Green + Near Infrared), has been used to demarcate flooded areas (Jain et al., 2005).

In order to include uncertainty arising from the choice of image and image processing technique in the flood maps, we followed the general principle of the possibility of inundation maps proposed by Schumann et al. (2009). However, unlike that study we did not have access to multiple, simultaneous images . As the differences in digital image processing techniques are the main reason for variation in the output binary flood maps, we added all four binary maps pixel-by-pixel and divided the summed map by 4 to produce a simple possibility of inundation map (Fig 4), where the pixels represent discrete probabilities (Table 1). Finally, the inundation maps derived by unsupervised classification of the LISS III image and supervised classification of the Landsat 5 TM image were used as deterministic binary inundation maps (Fig 5).

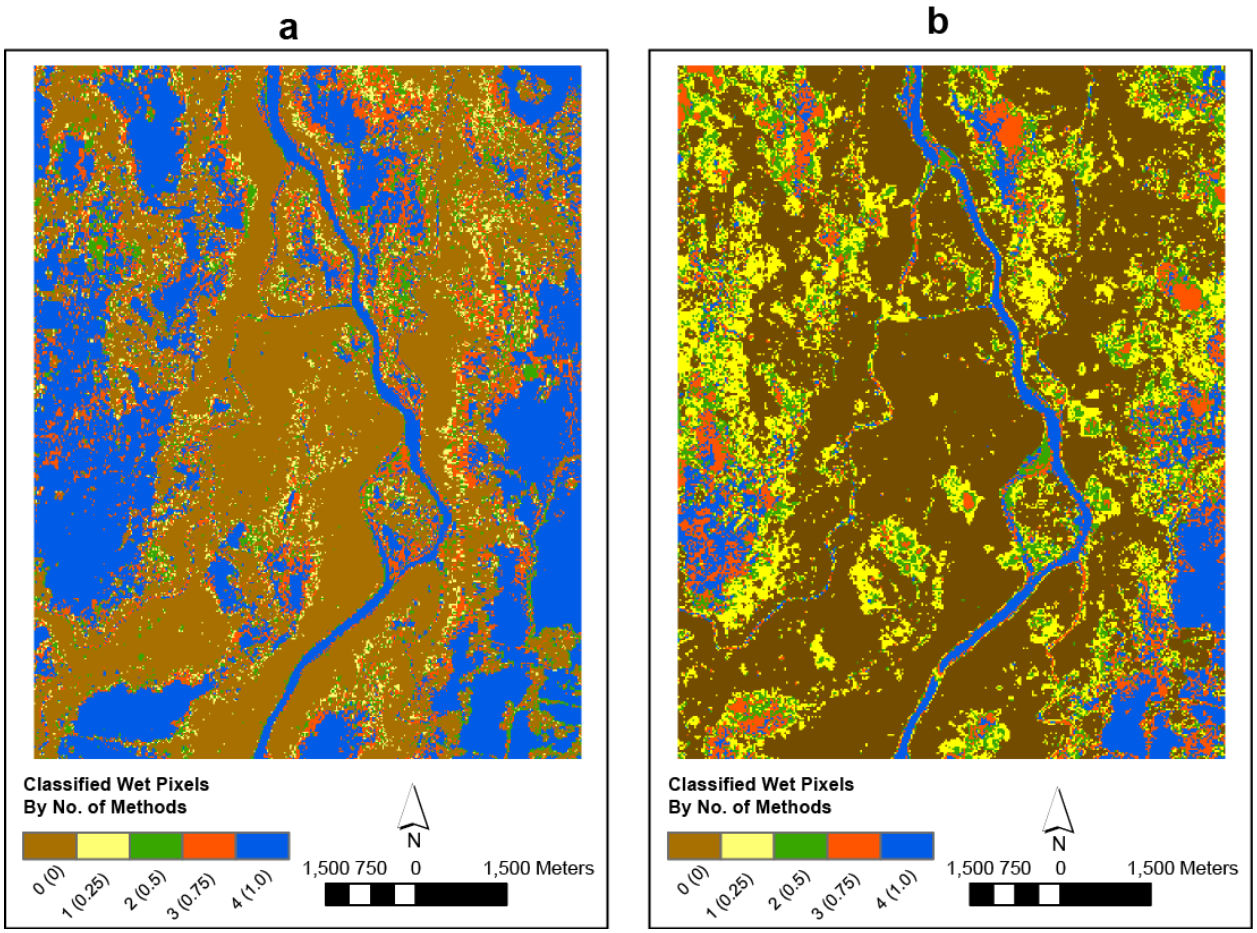

Fig 4 Possibility of inundation maps derived from (a) the LISS-III image on 12 Septemberand (b) the Landsat 5 TM image on 15 September, 2009.

Table1 The pixel values and their actual meanings in the possibility of inundation maps.

Pixel Value	**Characteristics**
0	Pixels not classified as flooded by any of the four methods
0.25	Pixels classified as wet by one of the four methods
0.50	Pixels classified as wet by two of the four methods
0.75	Pixels classified as wet by three of the four methods
1	Pixels classified as wet by all four methods

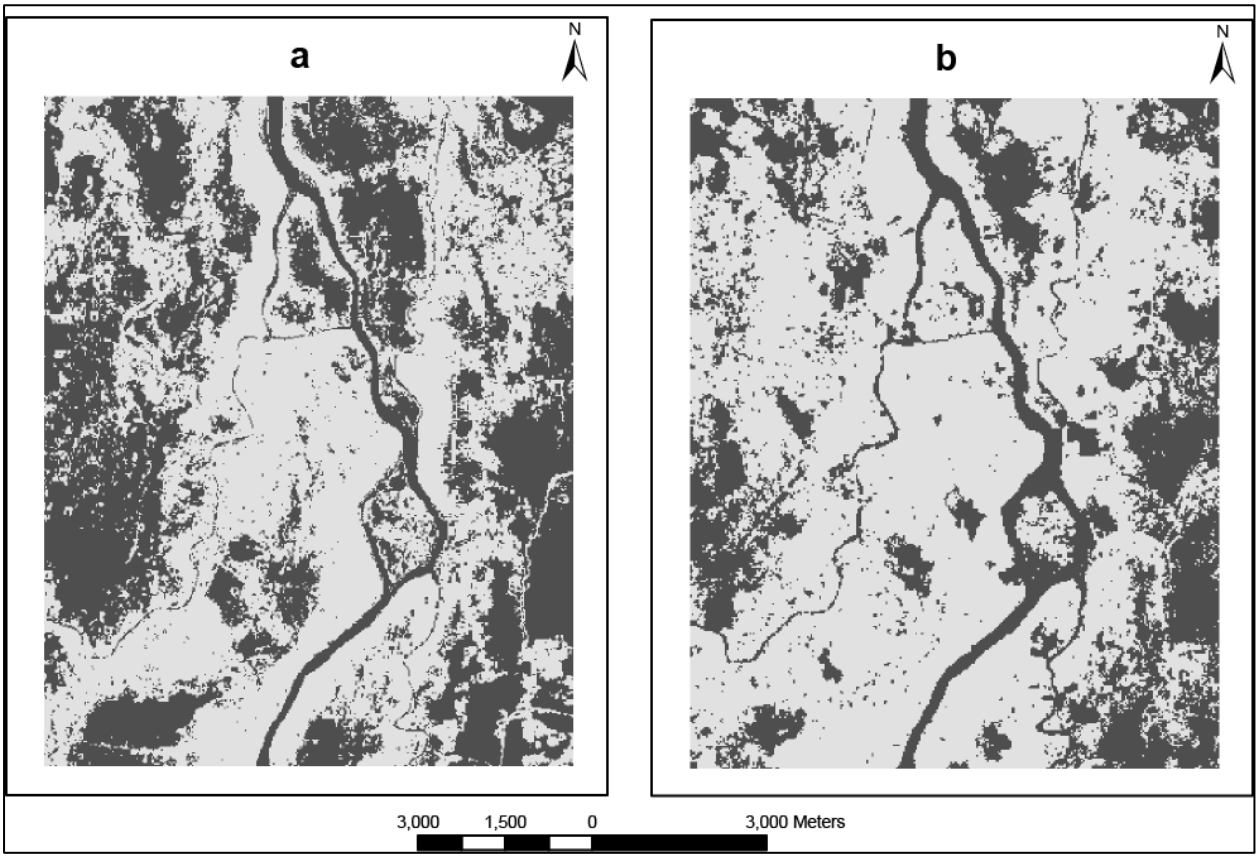

Fig 5 Deterministic inundation maps derived by (a) unsupervised classification of the LISS-III image on 12 Septemberand (b) supervised classification of the Landsat 5 TM image on 15 September, 2009.

3.3 Setting up the inundation model

TELEMAC2D is a fully 2D finite element inundation model that solves second-order depth-averaged partial differential equations for free surface flow. A full description of the equations can be found in Hervouet and Van Harn (1996). An unstructured finite element mesh was created using Blue Kenue software (NRC Canadian Hydraulics Centre, 2014). We ensured that the mesh had approximately equilateral elements on the floodplain to minimize mass balance error, and had variable element size to enable concentration of computational resources as necessary. Smooth transitions were imposed between smaller element sizes over channel and other narrow features and larger element sizes over the floodplain to increase model stability. The node spacing in the finite element mesh roughly followed the density of points in the hybrid terrain data.

3.4 Setting up the GLUE-based uncertainty assessment experiment

The model was composed of 674901 nodes and 1349048 elements and took 50 hours to complete one simulation run for the 186 hour flood event using a PC with an Intel i7 8-core processor. Clearly, standard workstations are not capable of performing numerous Monte Carlo-type simulations for this kind of model, but TELEMAC2D is easily adapted to parallel computing architecture used in high performance computing (HPC) hardware.

We used the HPC facility at Durham University to perform our Monte Carlo simulations. Five parameters were identified as the primary sources of uncertainty (Table 2): 1) Manning's n for the channel at the gauging site (InQnch) for converting stage into discharge, 2) Manning's *n* for the floodplain at the gauging site (InQnfp) for converting stage into discharge, 3) a global Manning's *n* for the channel (nch), 4) a global Manning's *n* for the floodplain (nfp), and 5) the solver used for the system of equations (slv). Parameters 1 and 2 were directly related to the amount of water entering the model domain, with higher roughness resulting in lower discharge for the same stage. Parameters 3 and 4 are conventional sources of uncertainty across the model space. Parameter 5 has impacts on both the computational time and the model solution. The four solvers used were 1) the conjugate gradient method (CG), 2) the conjugate residual method (CR), 3) the normal equation method (NE), and 4) the squared conjugate gradient method (SCG). The Monte Carlo approach for deriving numerous flood-extent maps from TELEMAC2D model outputs is presented in Fig 6.

Table 2 Range of variation of the uncertain parameters applied in the Monte Carlo simulation.

Parameter	**Range**	**Increment**	**No. of choices**
InQnch	0.026-0.038	0.001	13
InQnfp	0.030, 0.035, 0.038	-	3
nch	0.024-0.038	0.001	15
nfp	0.030, 0.035, 0.038	-	3
Solver	CG, CR, NE, SCG	-	4

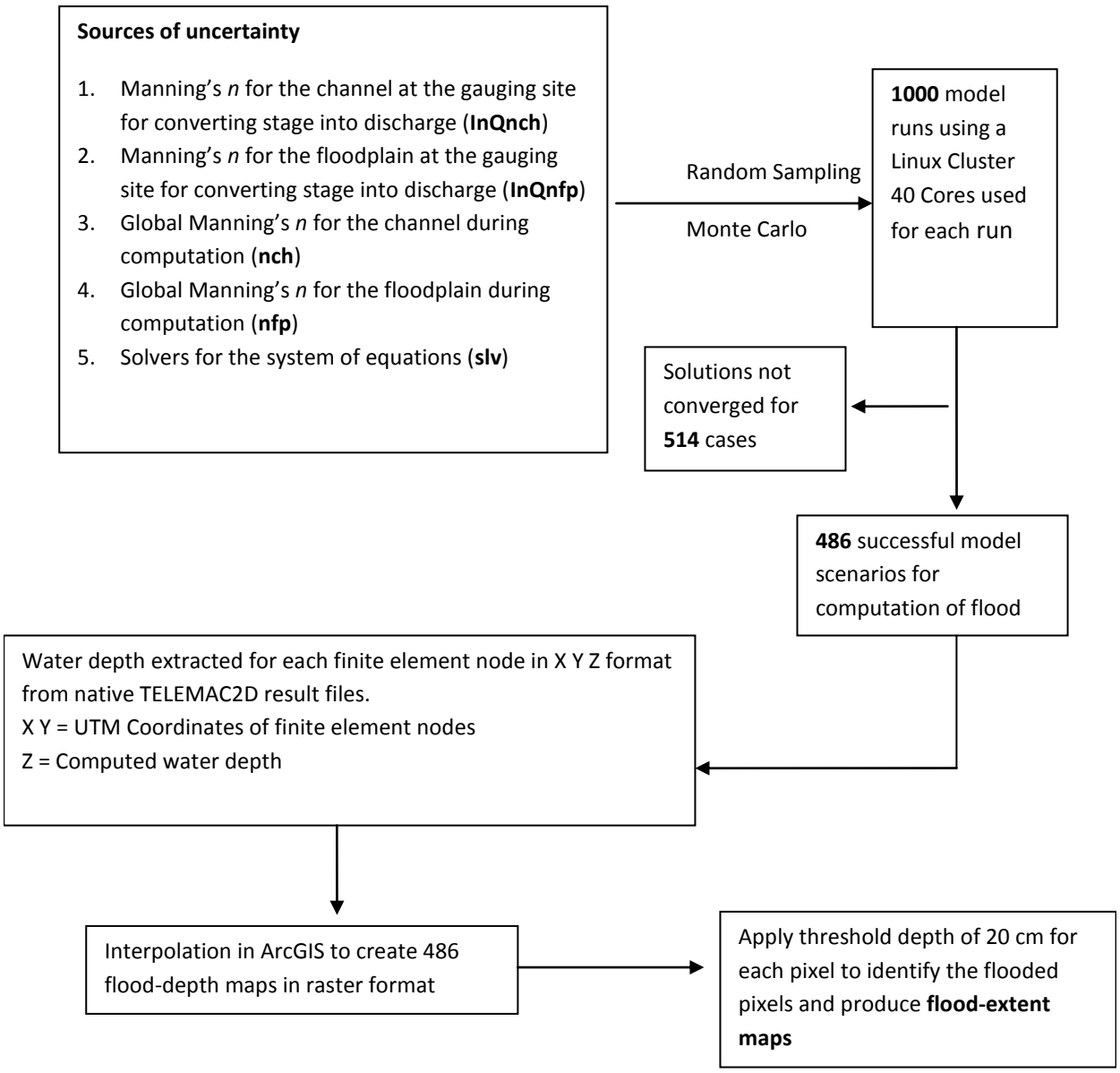

Fig 6 Flow diagram showing the methodology of deriving multiple flooding scenarios for uncertainty assessment using Monte Carlo principles.

We used a GLUE-based framework to quantify the predictive uncertainty in TELEMAC2D outputs by employing two types of observed inundation maps for conditioning the likelihood weights. The deterministic binary inundation maps (Fig 5) were used following the method proposed by Aronica et al. (2002), and the possibility of inundation maps (Fig 4) were used to incorporate uncertainty in satellite-observed flood extents following the methodology of Di

Baldassarre et al. (2009). As both approaches produce probability maps of predicted inundation, we compared the differences in their spatial patterns.

First, the performance of TELEMAC2D model was measured against the deterministic inundation maps with the objective function of Horritt and Bates (2001):

$$F = (O_w \cap M_w / O_w \cup M_w) \times 100 \quad (2)$$

where O_w is the number of observed wet pixels and M_w is the number of modelled wet pixels. A likelihood weight L_i was assigned to each successful Monte Carlo simulation i using

$$L_i = F_i - \text{Min}(F) / \text{Max}(F) - \text{Min}(F) \quad (3)$$

where F_i is the performance score of the ith simulation, and Max(F) and Min(F) are the maximum and minimum performance scores in the ensemble.

The weighted average flood state X_j for the jth computational cell was derived as

$$X_j = \frac{\sum_i L_i m_{ij}}{\sum_i L_i} \quad (4)$$

where m_{ij} is the model output for the jth cell, which takes a value of 1 for wet and 0 for dry. Applying Equation 4 to all cells yields the probability of predicted inundation map. The entire process was automated using MATLAB.

Second, following Di Baldassarre et al. (2009), we used a reliability diagram (Horritt, 2006), where for each simulation i we counted the number of simulated wet cells falling in each of the probability regions in the possibility of inundation map (0, 0.25, 0.5, etc.). Horritt (2006) argued that the reliability diagram of a perfectly accurate model would result in a 1:1 relationship between the probability (in our case the figures in the possibility of inundation map) and the model proportion (the proportion of modelled wet cells in that probability region). The accuracy of any given simulation run can be measured by calculating the RMSE deviation from that 1:1 line. For each simulation, the model proportion for the probability regions (p_j) of 0, 0.25, 0.50, 0.75 and 1 were calculated. Then, we derived the RMSE as the deviation from the ideal relationship between the possibility of inundation and model proportion (Fig. 7).

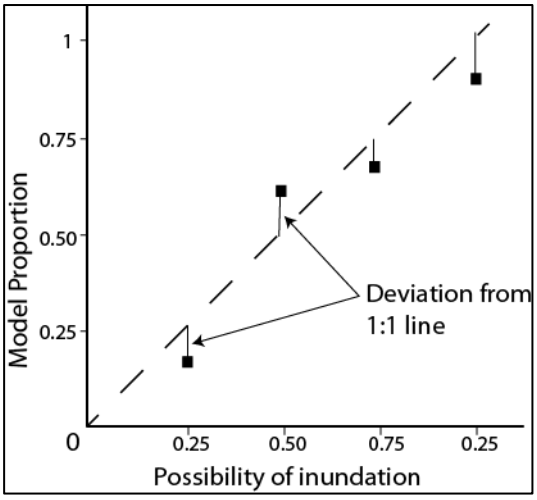

Fig 7 A schematic scatter diagram of model proportion and possibility of inundation. The 1:1 line representing a perfect model is shown with the dashed line.

A MATLAB routine was developed to perform this task for all the successful Monte Carlo simulation runs. The RMSE for each simulation was weighted by the number of cells in that class, ignoring the dry areas where $p_j = 0$.

The likelihood value (L_i) for each simulation was derived from the RMSE values as

$$L_i = \text{Max(RMSE)} - \text{RMSE}_i \,/\, \text{Max(RMSE)} - \text{Min(RMSE)} \qquad (5)$$

where Max(RMSE) and Min(RMSE) are the maximum and minimum RMSE values for all successful Monte Carlo simulation runs. The weighted average flood state for each cell was calculated with Equation 4, yielding a flood uncertain inundation map which illustrates the predictive uncertainty in the modelled inundation map derived from uncertainties in the observed flood extent.

Following Di Baldassarre et al. (2009), we computed a quantity D_j for model state 1 in order to investigate the difference between the possibility of inundation map and the flood uncertain inundation map. For the jth computational cell the quantity D_j was computed as the flood uncertain inundation figure minus the possibility of inundation figure. However, unlike Di Baldassarre et al. (2009) we did not consider all cells in the model domain for computing D_j as there were many dry cells (value = 0) in both flood uncertain inundation map and possibility of inundation map. Hence, a direct subtraction would result in a large number of spurious 0 values

that would falsely indicate a condition of little bias. In order to resolve this problem we ignored all cells that had a value of 0 in the possibility of inundation and flood uncertain inundation maps, so that the 0 values of D_j correctly depicted a scenario of perfect non-bias.

4 Results

More than 51% of the total model runs failed, 78% of which were due to the use of the NE solver. After discounting the NE solver simulations, we found that the percentage of model failure was approximately 4 times higher (up to ~ 80%) for a low channel roughness value of 0.024 compared to typical values of 0.029-0.035 for straight sand-bed rivers (Chow, 1959).
Fig 8 indicates the performance of the Monte Carlo simulations against the deterministic inundation maps in relation to four of the five uncertain parameters; note that performance was not sensitive to the floodplain Manning's n values at the inflow hydrograph (InQnfp), so this parameter is not shown. Considerable equifinality for all the uncertain parameters was noticed, indicating that similar accuracy in the predicted output was achieved using a range of values within each parameter. Despite this, Fig 8a illustrates that a lower roughness coefficient for the channel (0.026 to 0.030) generally had less cases with poor model performance.
None of the cases that used higher roughness coefficients (0.035 - 0.038) attained a goodness-of-fit of more than 0.36. However, this trend is not found for InQnch at model state 2, when the river level was down to almost the pre-flood level (Fig 3). The performance of the model at state 2 was quite poor with a maximum goodness-of-fit figure of 0.28, but the model showed less equifinality and the advantage of using a smaller InQnch value is evident (Fig 8e).

The channel Manning's roughness coefficient (nch) shows some equifinality, but a trend of higher goodness-of-fit against deterministic observed inundation maps with higher nch values is evident in both model states (Fig 8b, f). The model outputs were found to be completely insensitive to the floodplain Manning's roughness coefficient (nfp) and to the choice of solver in TELEMAC2D at both states (Fig 8c-d, g-h). The probability of inundation maps (Fig 9) show that at both model states the inundated surface is patchy and not necessarily found adjacent to the channels. A substantial portion of the total area under flooding has been modelled as inundated in majority of the Monte Carlo realisations.

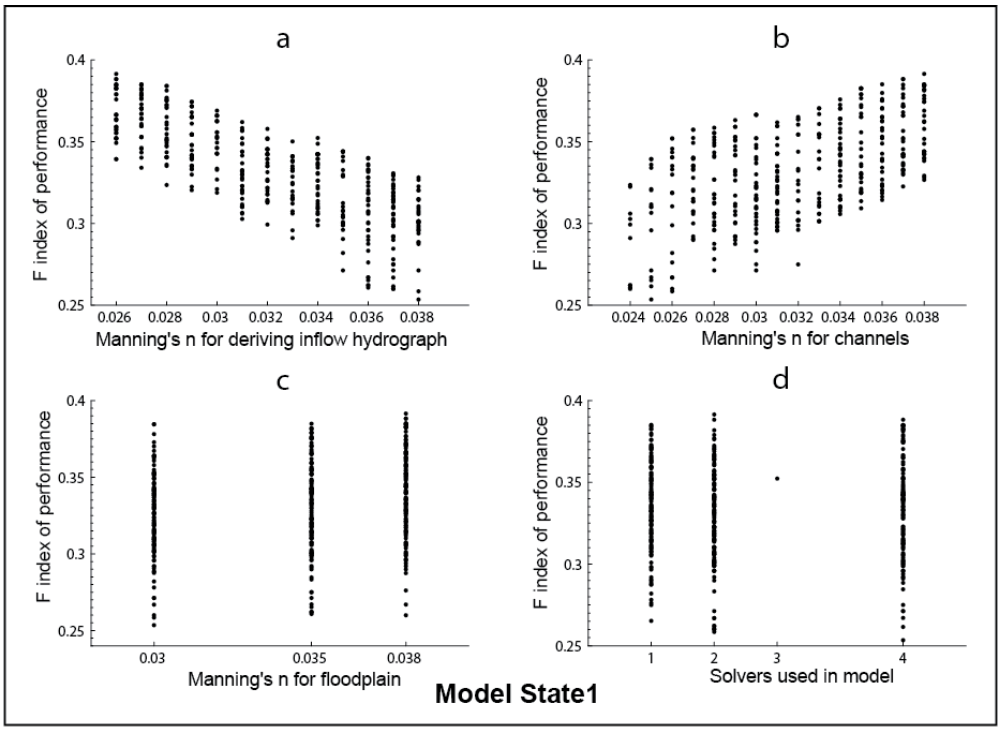

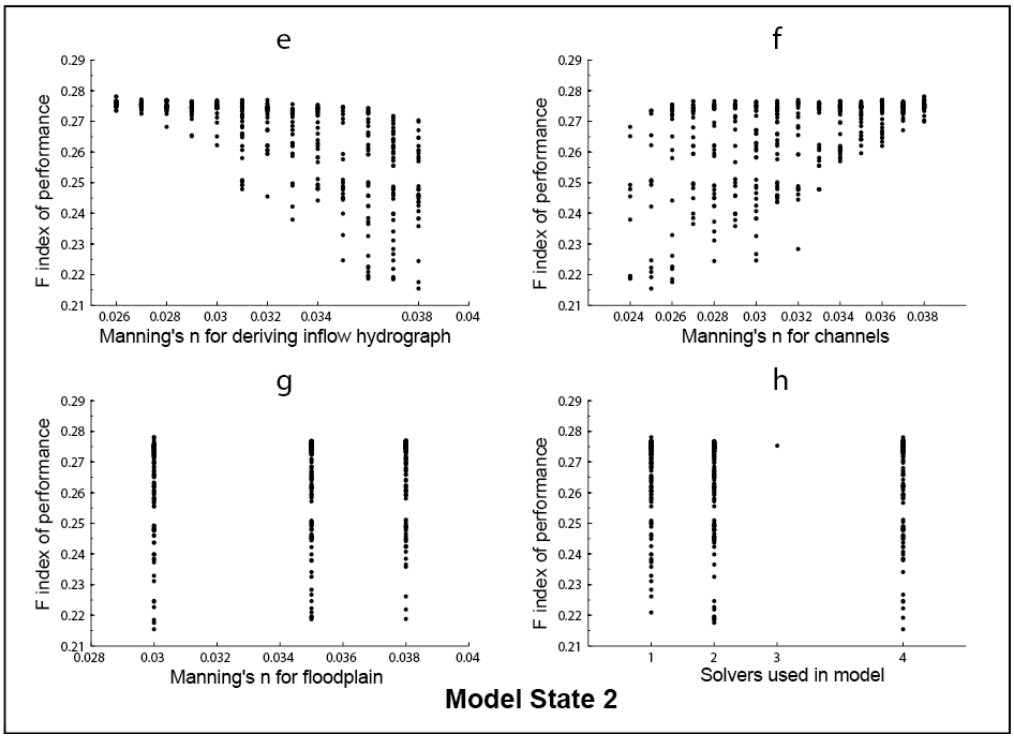

Fig 8 Dotty plots showing the performance of the TELEMAC2D model at model state 1 (panels a-d) and model state 2 (panels e-h) in relation to (a, e) channel Manning's n for deriving the inflow hydrograph from stage data (InQnch), (b, f) Manning's n for the channels (nch), (c, g) Manning's n for the floodplain (nfp), and (d, h) the solver used for solving the system of equations.

The flood uncertain inundation maps created by incorporating the uncertainty of satellite-observed flood extents show similar patterns as the deterministic probability of inundation maps (Fig 9) and are not presented. However, there are systematic spatial differences in the likelihood of flooding in the two maps. To examine the nature and causes of these differences at model state 1, the probability of inundation map was subtracted from the flood uncertain inundation map to produce Fig 10. The differences are most pronounced in three areas: 1) at the periphery of the areas with a very high likelihood of being modelled as flooded, 2) where complex hydraulic processes take place such as the river island at the centre, and 3) areas in the extreme south and the northeast corner, where the possibility of inundation map (Fig 4a) indicates lower level of confidence in the observed inundation data. In general, these areas fall outside the highly likely modelled inundation zones, and have higher uncertainty in the observed inundation data.

The histogram of D_j values (Fig 11) was created to test the tendency of bias in the model output for model state 1. It shows a bimodal distribution with one peak around 0 and another around -1. The peak around 0 is a sign of little or no bias between the modelled and observed probability of inundation. The other peak at -1 is an indication that a substantial portion of the observed flooded area (1 in the possibility of inundation map) was simulated as dry by the model (0 in modelled output), indicating systematic underestimation of the flooded area.

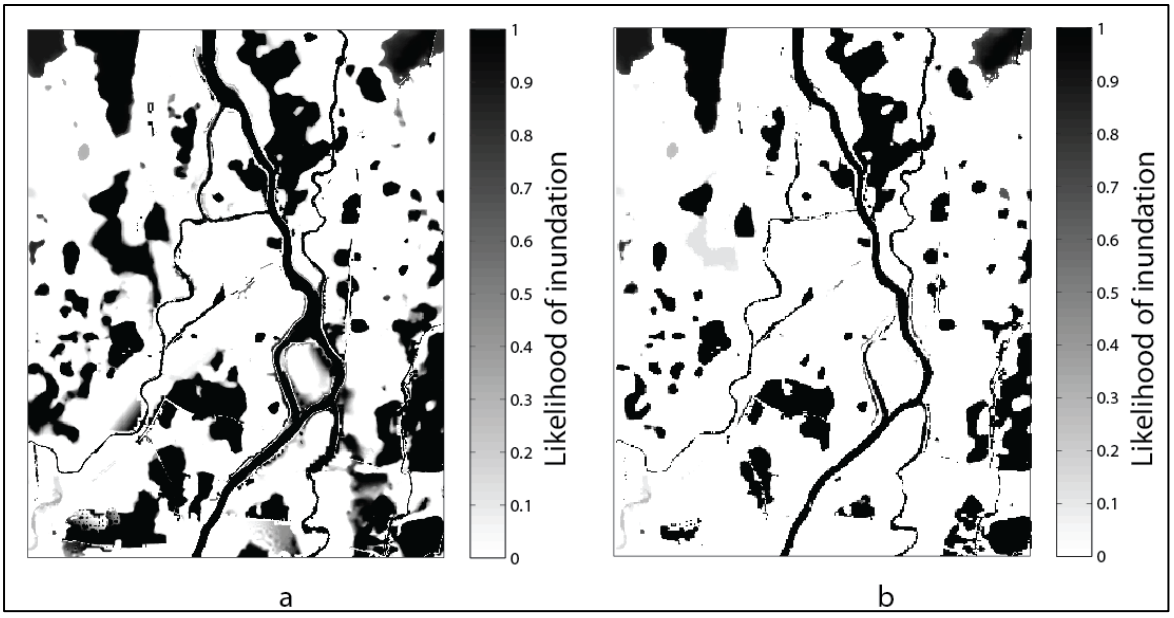

Fig 9 Probability of inundation maps derived from the deterministic binary inundation maps showing the likelihood of the model predicted inundation area on (a) model state 1 and (b) state 2.

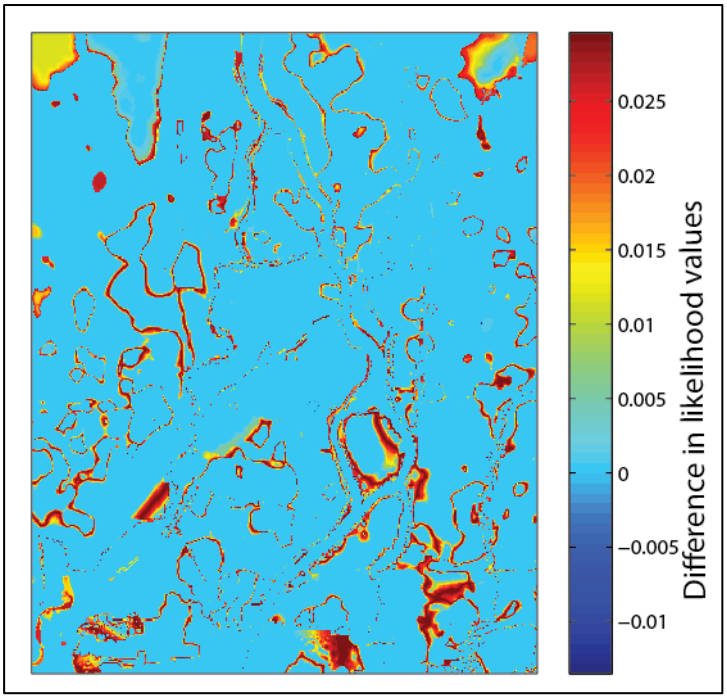

Fig 10 Difference in probabilities derived by subtracting probability of inundation from flood uncertain inundation values for model state.

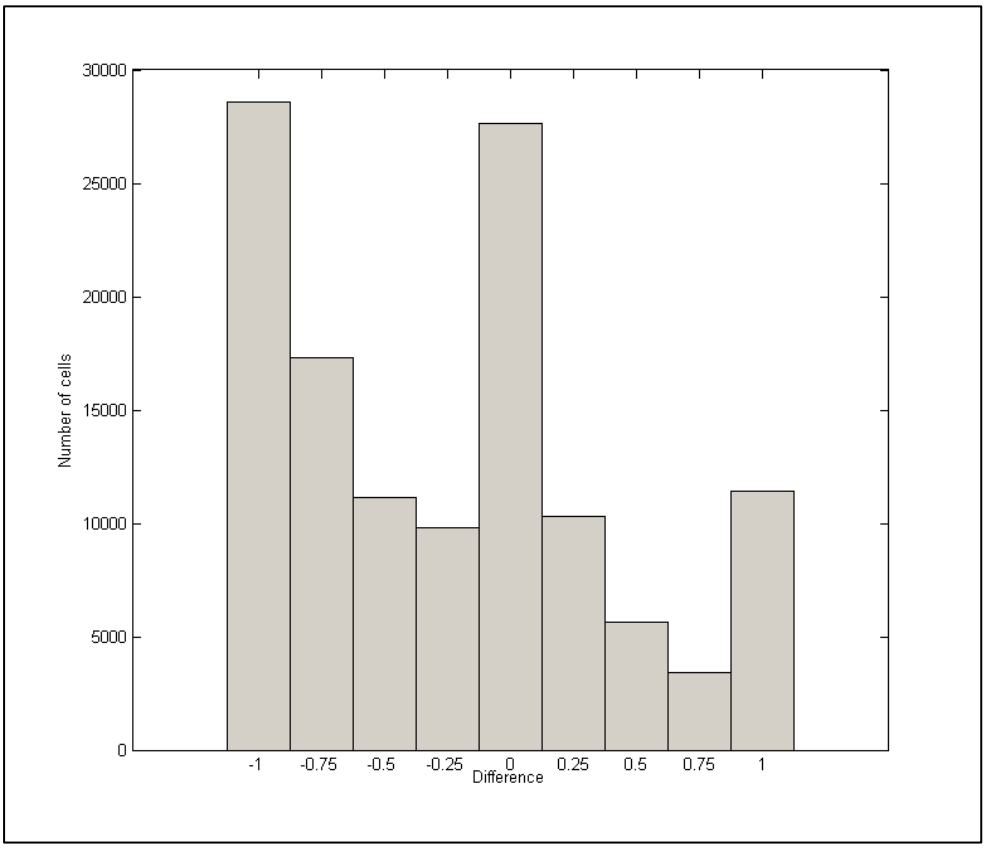

Fig 11 Histogram of Dj values. The peak around 0 shows a lack of bias in the flood uncertain probability map but the peak around -1 illustrates that a substantial portion of the observed flooded area is underpredicted by the model.

5 Discussion

InQnch and nch values affected the performance of TELEMAC2D in different ways. An increase in the value of InQnch results in less discharge for a given river stage, and the overall accuracy of predictions for model state 1 decreased steadily with a reduction in the inflow of water in the model domain (Fig 8a). At a later stage of the flood (model state 2), however, the model was found to be less sensitive to the variation of inflow discharge and performed with equal accuracy for a range of inflow hydrographs produced by different values of InQnch (Fig 8e). There are two possible reasons for this model behaviour. First, at very high river stages in state 1, slight differences in the channel roughness coefficient led to considerable increases in the computed discharge values. A decrease in the supply of water at the inlet possibly amplified the problem of underprediction, particularly in the western section of the model domain, resulting in decline in the model performance score. Secondly, during the model state 2 when stage was well below bankfull, the change in discharge values had little impact on the modelled flood extent maps. At this stage the model efficiency mostly depends on the strength of its wetting and drying algorithm which is also very much dependent on the resolution and accuracy of the input terrain data.

The areas represented in dark tones in the probability of inundation maps (Fig 9) do not imply a high actual probability of inundation, but are instead highly likely to be modelled as inundated by the existing modelling setup. A comparison of Fig 9 with Fig 5 reveals that the drying process of the model could not fully reproduce the actual pattern of drying between the two stages of this flooding event. The model showed little sensitivity to declining inflow from 12 to 15 September when simulating inundation at the extreme upper portion of the image. This was probably due to the coarse quality of the terrain data, especially over the farmlands which were mostly derived from the SRTM DEM. The existence of large flat areas with small variations in relief was probably responsible for the poor performance of TELEMAC2D in terms of draining shallow water from parts of the floodplain. This overestimation of the flooded area is also manifested in Fig 11. It shows a considerable number of pixels with a D_j value of 1, indicating that they were modelled as wet but not classified as inundated using any of the image processing techniques.

Running numerous Monte Carlo simulations in TELEMAC2D is a computationally intensive task, and therefore it is beneficial to avoid unstable model runs that may use considerable

computational resources. We found that low nch values had a high incidence of instability and that their use did not lead to best model performance, at least near the peak of the flood (Fig 8b). We acknowledge that model stability depends on the complex interplay between the chosen parameter space, model inputs and the physical characteristics of the model domain. Due to these factors every inundation modelling experiment will have a unique pattern of model stability. However, a small but representative subset of the entire range of parameters may be used to perform some pilot runs to understand the incidence of instability with reference to the choice of parameter space.

6 Conclusion

We undertook a GLUE-based uncertainty assessment of simulated flood extents at two stages of the descending limb of a flood hydrograph using TELEMAC2D. The uniqueness of this study lies in adapting the existing techniques of uncertainty assessment for data-poor regions. The spatial distribution of uncertainties in an area with anabranching channels depends on 1) the state of the flood under consideration in relation to the occurrence of the flood peak, and 2) the amount of consistent bias in the model output arising from the sparse nature of the model inputs . We observed that portions of the modelled flood-extent maps were less sensitive to changes in important inputs, such as the inflow hydrograph. This type of model behaviour can be attributed to the lack of detailed floodplain topography for portions of the model domain.

The probabilistic observed data have an increased computational cost when compared to deterministic flood maps. However, the resulting uncertainty estimation is not significantly different and we therefore recommend the use of deterministic flood-extent maps for uncertainty assessment in data-sparse study sites. The uncertainty assessment of a fully 2D finite element model has never been attempted with sparse inputs in areas of multiple channel bifurcations. Hence, the findings of this paper will be helpful in judging the limitations of a similar modelling task where ideal model inputs and validation data do not exist.

Acknowledgements

The authors would like to thank Dr. Henk Slim of the Computing and Information Services (CIS), Durham University and Dr. Charles Moulinec of the Science and Technology Facility (STFC) Council, UK for their help in installing TELEMAC2D model in the high performance computing cluster of Durham University.

Reference

Adhikari P, Hong Y, Dauglas KR, Kirschbaum DB, Gourley J, Adler R, Brakenridge GR. (2010) A digitized global flood inventory (1998-2008): compilation and preliminary results. Natural Hazards 55: 405-422.

Aronica G, Bates PD, Horritt MS (2002) Assessing the uncertainty in distributed model predictions using observed binary pattern information with GLUE. Hydrological Processes 16: 2001-2016.

Bales JD and Wagner CR (2009) Sources of uncertainty in flood inundation maps, Journal of Flood Risk Management 2:139-147.

Bates PD (2012) Integrating remote sensing data with flood inundation models: how far have we got? Hydrological Processes 26: 2515-2521.

Beven KJ, Binley AM (1992) The future of distributed models: model calibration and uncertainty prediction. Hydrological Processes 6: 279–298.

Chow VT (1959) Open Channel Hydraulics. McGraw-Hill, New York.

Cook A, Merwade V (2009) Effect of topographic data, geometric configuration and modelling approach on flood inundation mapping. Journal of Hydrology 377: 131-142.

Di Baldassarre G, Claps P (2011) A hydraulic study on the applicability of rating curves. Hydrology Research 42:10-19.

Di Baldassarre G, Montanari A (2009) Uncertainty in river discharge observations: a quantitative analysis. Hydrology and Earth System Sciences 13: 913-921.

Di Baldassarre G, Schumann G, Bates PD, Freer JE, Beven KJ (2010) Flood-plain mapping: a critical discussion of deterministic and probabilistic approaches. Hydrology Science Journal 55(3): 364-376.

Di Baldassarre G, Schumann G, Bates PD (2009) A technique for the calibration of hydraulic models using uncertain satellite observation of flood extents. Journal of Hydrology 367: 276-282.

Herschey RW (1998) Flow measurement. In: Herschey RW (ed.), Hydrometry: principles and practices, Wiley, Chichester, pp 9–83

Hervouet J-M, Van Harn L (1996) Recent advances in numerical methods for fluid flows, In: Anderson MG, Walling DE, Bates PD (ed) Floodplain Processes, Wiley, Chichester, pp 183 – 214.

Horritt MS (2000) Calibration of a two-dimensional finite element flood flow model using satellite radar imagery. Water Resources Research 36: 3279-3291.

Horritt MS, Bates PD (2001) Effects of spatial resolution on a raster based model of flood flow. Journal of Hydrology, 253(1), 239-249.

Horritt MS (2006) A methodology for the validation of uncertain flood inundation models. Journal of Hydrology 326: 153-165.

Jain S, Saraf A, Goswami A, Ahmad T (2006) Flood inundation mapping using NOAA AVHRR data. Water Resources Management 20(6): 949-959.

Jain SK, Sing RD, Jain MK, Lohani AK (2005) Delineation of flood prone areas using remote sensing techniques. Water Resource Management 19: 333-347.

Jung Y, Merwade V (2012) Uncertainty Quantification in Flood Inundation Mapping Using Generalized Likelihood Uncertainty Estimate and Sensitivity Analysis. Journal of Hydrologic Engineering 13: 608-620.

McFeeters SK (1996) The use of Normalised Difference Water Index (NDWI) in the delineation of open water features. Int. J. Remote Sens. 17(7): 1425–1432.

Merz B, Kreibich H, Apel H (2008) Flood risk analysis: uncertainties and validation. Österreichische Wasser- und Abfallwirtschaft 60(5): 89-94. doi: 10.1007/s00506-008-0001-4

Montanari A (2006) What do we mean by uncertainty? The need for a consistent wording about uncertainty assessment in hydrology. Hydrological Processes 21: 841-845.

NRC (National Research Council Canada), Canadian Hydraulics Centre, Blue Kenue: Software tool for hydraulic modellers

http://www.nrc-cnrc.gc.ca/eng/solutions/advisory/blue_kenue_index.html Accessed, 10 January 2014

Pappenberger F, Beven K, Horritt M, Blazkova S (2005) Uncertainty in the calibration of effective roughness parameters in HEC-RAS using inundation and downstream level observations. Journal of Hydrology 302: 46-69.

Patro S, Chatterjee C, Singh R, Raghuwanshi NS (2009) Hydrodynamic modelling of a large flood-prone river system in India with limited data. Hydrological Processes. 23:2774-2791.

Sanyal J**,** Carbonneau P, Densmore AL (2014) Low-cost flood inundation modelling at a reach scale with sparse data in the Damodar river basin, India, Hydrological Sciences Journal. doi: 10.1080/02626667.2014.884718

Schumann G, Di Baldassarre G, Bates PD (2009) The utility of spaceborne radar to render flood inundation maps based on multialgorithm ensembles. IEEE Transactions on Geosciences and Remote Sensing 47(8): 2801–2807.

Stephens EM, Bates PD, Freer JE, Mason DC (2012) The impact of uncertainty in satellite data on the assessment of flood inundation models. Journal of Hydrology 414-415: 162-173.